

Article

Influence of Higher Stabilization Temperatures on the Microstructure and Mechanical Properties of Austenitic Stainless Steel 08Ch18N10T

Tomáš Janda ^{1,*}, Štěpán Jeníček ¹, Ludmila Kučerová ¹, Radek Leták ¹, Dagmar Jandová ² and Hana Jirková ³

¹ Regional Technological Institute, Faculty of Mechanical Engineering, University of West Bohemia, Univerzitní 8, 301 00 Pilsen, Czech Republic; jeniceks@fst.zcu.cz (Š.J.); skal@fst.zcu.cz (L.K.); letak@fst.zcu.cz (R.L.)

² New Technologies Research Centre, University of West Bohemia, Teslova 1198/9, 301 00 Pilsen, Czech Republic; jandova@ntc.zcu.cz

³ Department of Material and Engineering Metallurgy, Faculty of Mechanical Engineering, University of West Bohemia, Univerzitní 8, 301 00 Pilsen, Czech Republic; hstankov@fst.zcu.cz

* Correspondence: jandat@fst.zcu.cz

Abstract: Precipitation strengthening in titanium-stabilized austenitic stainless steels can improve the hot yield strength, as requested, e.g., for nuclear industry applications. The resulting properties depend mainly on the parameters of the heat treatment and previous forming. The influence of the heat treatment parameters on the development of the microstructure and mechanical properties was determined for steel 08Ch18N10T (GOST). Solution annealing and stabilization with different temperatures and holds were performed on the steel, which was, in delivered condition, stabilized at 720 °C. Heat-treated samples were subjected to static tensile testing at room temperature and at 350 °C, microstructural analysis using light, scanning electron and transmission electron microscopy focused on precipitates, and HV10 hardness testing. The strengthening mechanism and its dependence on the stabilization parameters are described. The results of the experiment show the influence of the state of the input material on the final effect of heat treatment—repeated heat treatment achieved lower-strength characteristics than the initial state, while almost all modes showed above-limit values for the mechanical properties. Stabilization temperatures of 720 to 800 °C were found to be optimal in terms of the achieved hot yield strength. At higher temperatures, slightly lower strengths were achieved, but at significantly shorter dwell times.

Keywords: heat treatment; precipitation strengthening; titanium carbide; hot yield strength; austenitic stainless steel



Citation: Janda, T.; Jeníček, Š.; Kučerová, L.; Leták, R.; Jandová, D.; Jirková, H. Influence of Higher Stabilization Temperatures on the Microstructure and Mechanical Properties of Austenitic Stainless Steel 08Ch18N10T. *Metals* **2023**, *13*, 975. <https://doi.org/10.3390/met13050975>

Academic Editor: Atef Saad Hamada

Received: 11 April 2023

Revised: 5 May 2023

Accepted: 13 May 2023

Published: 18 May 2023



Copyright: © 2023 by the authors. Licensee MDPI, Basel, Switzerland. This article is an open access article distributed under the terms and conditions of the Creative Commons Attribution (CC BY) license (<https://creativecommons.org/licenses/by/4.0/>).

1. Introduction

The heat treatment (HT) of austenitic stainless steels is a current problem not only in research but also in industrial practice. Due to their properties, these steels are widely used in nuclear engineering and the food and petrochemical industries. In addition to good mechanical and technological properties (weldability, formability), austenitic stainless steels are characterized by excellent corrosion resistance in normal environments and conditions. The weakness of the common grades is, however, their susceptibility to intergranular corrosion when exposed to higher temperatures and more aggressive environments [1]. If the steel is sensitized in the temperature range of 425–870 °C [2] (or 500–950 °C [3]), chromium carbides can precipitate along the grain boundaries and cause local depletion of the steel by chromium [2]. This problem can be solved either by reducing the carbon content of the steel or, for even better effect, by stabilizing the steel with an element with high carbon affinity (Ti or Nb) [1]. During HT (so-called stabilization), the excess carbon is excluded in the form of stable carbides or carbonitrides of the stabilizing element, and thus, further precipitation of the chromium carbides is prevented. The material stabilized in this

way may also show some increase in the values of its mechanical properties depending on the processing parameters. This is particularly useful for parts operating at higher temperatures due to the high thermal stability of the precipitates.

Many research papers discuss the heat treatment of stabilized austenitic stainless steels. Publications have very often dealt with the HT of parts after welding [4–7], corrosion resistance (especially intercrystalline corrosion) [8–11], fatigue properties [12–14], or the mechanical properties of commercial steel AISI321 [15–17]. However, what is not very common in the literature is the issue of the HT of stabilized grades in order to increase their mechanical characteristics, especially the cold and hot yield strength (YS) and ultimate tensile strength (UTS) [18]. There is a particular lack of papers concerning non-commercial steel 08Ch18N10T according to GOST standards, developed especially for the needs of nuclear engineering, and which is subject to higher demands for its mechanical properties and micropurity. Some publications have also studied the deformation behavior of AISI321 steel [19–22], rolling or forging conditions and their effect on the strain hardening of 08Ch18N10T steel, or the course of solution and stabilization annealing [23]. It is known that these forming operations have a certain effect on the production process of the steel. Although the importance of deformation hardening is not essential for the final hot yield strength (YS $^{350^{\circ}\text{C}}$; the achieved strengths decrease again very rapidly due to the high-temperature solution annealing), the influence of the deformation strengthening on the kinetics of the precipitation processes, and thus, the secondary hardening was proved.

The processes currently used for the production of 08Ch18N10T steel have been proven in practice but are time-consuming and costly. In particular, efforts are being made to shorten and streamline the stabilization mode (720 °C for 10 h). It can be assumed that the original parameters of the stabilization were probably designed to achieve the required mechanical properties even with lower-quality formed semi-finished products. If this assumption is correct, then the possibility of re-evaluating the processing parameters in the individual stages of production, and thus, streamlining the production process becomes possible.

The material after processing must have high corrosion resistance together with good hot mechanical properties, which makes the issue of the HT of such material complex, requiring a thorough knowledge of the processing methods and the processes taking place during the treatments. Therefore, it is important to check the influence of the parameters of the individual production operations and determine the significance of their effects (i.e., metallurgy, forming, heat treatment) on the desired increase in the YS. This article, therefore, focuses on the temperature and dwell time during stabilization annealing. As the stabilization temperature increases, the kinetics of the precipitation processes increase, so we can assume that a slight increase in the stabilization temperature makes it possible to achieve the desired precipitation hardening in a significantly shorter time. Since a higher stabilization temperature generally also favors corrosion resistance, this combination appears to be particularly advantageous. However, the morphology of the precipitates and other aspects are also important. In order to shorten the production process while reaching the prescribed YS $^{350^{\circ}\text{C}}$, it is necessary to obtain a comprehensive description and understanding of the processes taking place in the various stages of stabilization annealing, while also taking into account the previous processing history.

2. Experimental Methods

The austenitic stainless steel 08Ch18N10T stabilized with titanium (Table 1) was chosen as the experimental material. Due to its use in nuclear engineering, this steel has a prescribed micropurity control, which is governed by the GOST 1778–70 standard. The content, morphology, and distribution of titanium carbonitrides are also monitored. However, the limits, which are optimal in terms of the micropurity and corrosion resistance, may go against the requirements for the strength characteristics—with a higher carbon content, the rate of precipitation hardening increases [24]. Therefore, the carbon and titanium contents and their ratio are also closely monitored in this steel. The maximum

carbon content is 0.08%, while there must be at least five times more titanium, to a maximum of 0.7%. Furthermore, the minimum required cold and hot mechanical properties (Table 2), especially the $YS^{350^{\circ}\text{C}}$ (min. 177 MPa), are prescribed. Commercial equivalents of this steel are, for example, AISI 321 according to ASTM/ASME standards, and X6CrNiTi18-10 (1.4541) according to EN standards.

Table 1. Chemical composition of the material used for the experiment (08CH18N10T).

C (%)	Cr (%)	Ni (%)	Ti (%)	Mn (%)	Si (%)	P (%)	S (%)
0.05	17.75	10.05	0.43	1.8	0.52	0.024	0.014
Cu (%)	Mo (%)	V (%)	N (ppm)	W (%)	Co (%)	H (ppm)	
0.1	0.08	0.11	120	0.03	0.02	2.4	

Table 2. Prescribed mechanical properties: cold (according to GOST 1497-84), hot (according to GOST 9651-84); test specimen type IV-4, $l_0 = 50$ mm; shape of test specimens according to EN ISO 6892-1, annex D, test rod d 10 mm [25–27].

Evaluated Property	Requested Cold Mechanical Properties			Requested Hot Mechanical Properties	
	Dimension (mm)/Value			Evaluated Property	Value
	5–60	61–100	101–250		
YS (MPa)	min. 206		min. 196	$YS^{350^{\circ}\text{C}}$ (MPa)	min. 177
UTS (MPa)	500–750			$UTS^{350^{\circ}\text{C}}$ (MPa)	min. 353
A (%)	min. 40	min. 38		$A^{350^{\circ}\text{C}}$ (%)	min. 25
Z (%)	min. 50			$Z^{350^{\circ}\text{C}}$ (%)	min. 45

The processed semi-finished product was in the form of forged bars with a nominal diameter of 90 mm. The bars were a delivered solution annealed at 1020 °C for 110 min, subsequently cooled in water and stabilized at 720 °C for 600 min, cooled in air. With regard to the efficient use of the volume of material, the semi-finished product was cut using a water jet into smaller segments of about 45 × 20 × 110 mm (Figure 1). Two tensile specimens were produced from each segment after HT. However, this method deviates from the rules of the methodology for micropurity evaluation and mechanical testing (according to the relevant standards, samples are always taken in the longitudinal direction, in the case of the bars with a diameter of >50 mm at a minimum distance of a quarter of the diameter from the rod surface). Therefore, the following labeling of individual tensile bodies was introduced: OO (segment and sample from the edge of the rod), OS (edge sample, middle segment), SS (middle sample and segment).

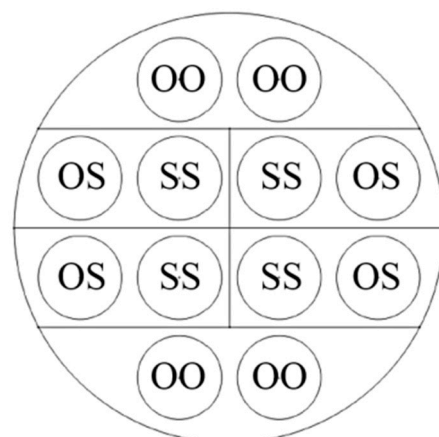


Figure 1. Cross-section of the bar \varnothing 90 mm—marking of the sampling points.

Thus, it was possible to monitor the influence of the sampling point in the cross-section of the rod on the development of the microstructure and mechanical properties. The selection of the segments for each HT mode was always the same—1 piece from each marking. It was proven (both on the samples after HT and in the initial state) that the proposed method of sampling did not significantly affect the results. The average values are presented in the graphs.

In order to determine the influence of the stabilization parameters on the mechanical properties and microstructure of 08Ch18N10T steel, segments with the approximate dimensions of $45 \times 20 \times 110$ mm, cut from the supplied semi-finished product $\varnothing 90$ mm, were heat-treated. A sequence was designed for the heat treatment of the experimental material, including solution annealing at 1020°C for 30 min, and water quenching and subsequent stabilization with variable parameters (temperatures from 720 to 900°C ; dwell times from 30 min to 15 h—Table 3). The heat treatment was performed in an atmospheric furnace. In order to determine only the effect of the solution annealing itself, a separate solution annealing at 1020°C with a holding time of 30 min (without stabilization) was also tested. During processing, the temperature of the semi-finished products was measured using K-type thermocouples (Omega engineering Inc., Norwalk, CT, USA) placed in the drilled holes. A stabilization temperature of 720°C was chosen in order to repeat the mode by which the supplied starting material was processed on the samples under laboratory conditions. Thus, it was possible to reliably compare this heat treatment mode with other modes.

Table 3. Proposed modes of heat treatment—stabilization of the samples.

Solution Annealing		Stabilization Temperature	Holding Time
1020 °C	30 min	720 °C	2.5/5/7.5/10/15 h
		800 °C	1/2.5/5/10 h
		850 °C	0.5/1/2.5/5 h
		900 °C	0.5/2.5 h

Samples for mechanical tests and metallographic analyses were then produced from the processed segments by turning. Microstructural analyses were performed using light (LM) and scanning electron microscopy (SEM). The key property observed for this steel is the hot YS $^{350^\circ\text{C}}$ (min. 177 Mpa). Achieving this value is problematic, especially in combination with good corrosion resistance and the associated requirements of micropurity. Therefore, standardized tensile tests were performed at 350°C , and at the same time, tests at room temperature (RT) were performed for comparison. Based on the results, 2 stabilization modes were selected for a detailed analysis of the precipitates and a study of the strengthening mechanism using diffraction analysis on thin films in a transmission electron microscope (TEM). These were samples with stabilization annealing at 800°C for 1 and 10 h. Higher stabilization temperatures and different dwelling times were chosen to monitor the effect of higher stabilization temperatures on the kinetics and behavior of the precipitates.

Metallographic samples for light and scanning electron microscopy were prepared by mechanical grinding and polishing, followed by chemical etching using 221 reagent (hydrofluoric acid/glycerin/nitric acid). Microstructure images and analyses were obtained using an Olympus light microscope (Olympus, Darmstadt, Germany) and a Zeiss EVO MA 25 scanning electron microscope (Zeiss, Oberkochen, Germany).

TEM analyses were performed using a JEOL JEM-2200FX microscope (JEOL, Tokio, Japan). Thin foils were ground using metallographic fine-grained papers down to a thickness of 0.1 mm. This was followed by electrolytic jet-polishing using 6% HClO₄ solution in methanol at a voltage of 23 V and a temperature of -60°C . TEM used an accelerating voltage of 200 kV.

The mechanical properties were determined by a standardized tensile test (CWICK ROELL 250, Haan, Germany) at 350°C and at RT. The tensile test at RT was performed

according to ISO 6892-1 (corresponds to GOST 1497-84) with strain rates of 0.00025 s^{-1} (up to the YS) and 0.0067 s^{-1} (after reaching the YS). A tensile test at $350 \text{ }^{\circ}\text{C}$ was performed according to ISO 6892-2 (corresponds to GOST 9651-84) with strain rates of 0.00007 s^{-1} (up to the YS) and 0.0014 s^{-1} (after reaching the YS). The dimensions of the test bars were $d = 10 \text{ mm}$, $l_0 = 50 \text{ mm}$ in both cases. The ultimate tensile strength (UTS), yield strength (YS), and elongation ($A_{5.65}$) were always measured. The test specimens for the tensile test were always taken from the edge (2 pcs) and the center (1 pcs) of the rod $\varnothing 90 \text{ mm}$. Thus, it was possible to check the influence of the sampling point and to find only negligible differences in the values measured for the samples from the center and the edge of the rod (according to the diagram in Figure 1).

3. Results

The mechanical tests were performed both on the initial delivered state and on the samples after the solution annealing and the various stabilization treatments. The results of these tests are given in Table 4. In addition, the measured values for the YS are plotted in summary graphs.

Table 4. Tensile test results.

Stabilization Temperature	Hold	Tensile Test at RT			Tensile Test at $350 \text{ }^{\circ}\text{C}$		
		UTS (MPa)	YS (MPa)	A (%)	UTS 350°C (MPa)	YS 350°C (MPa)	A 350°C (%)
Delivered condition		568	336	48	412	277	26
Annealed $1020 \text{ }^{\circ}\text{C}/0.5 \text{ h}$		557	294	50	398	233	27
$720 \text{ }^{\circ}\text{C}$	2.5 h	541	294	53	391	228	34
	5 h	543	300	54	395	241	32
	7.5 h	548	305	53	388	235	31
	10 h	551	306	52	392	241	31
	15 h	545	297	53	388	236	32
$800 \text{ }^{\circ}\text{C}$	1 h	548	297	54	390	238	30
	2.5 h	544	284	53	388	235	32
	5 h	541	286	53	381	227	29
	10 h	547	282	52	382	225	31
$850 \text{ }^{\circ}\text{C}$	0.5 h	550	293	53	389	233	30
	1 h	544	290	54	385	228	31
	2.5 h	545	287	53	385	230	30
	5 h	550	288	52	385	225	31
$900 \text{ }^{\circ}\text{C}$	0.5 h	542	282	54	384	220	32
	2.5 h	546	280	54	383	217	31

3.1. Room-Temperature Tensile Tests

The highest strength values (UTS = 336 MPa, YS = 277 MPa) and, at the same time, the lowest elongations (48%) were measured on a sample of the supplied initial state (IS). In comparison to the initial state (568 MPa), the reprocessed material reached lower values of YS both in the annealed state and after stabilization (Figure 2). The decrease in the YS caused by solution annealing (from 336 to 294 MPa for a 30-min dwell time) was compensated only by longer holds at a stabilization temperature of $720 \text{ }^{\circ}\text{C}$, but very slowly. The maximum YS (305 MPa) was found after 7.5 and 10 h dwell times. The longest holding time of 15 h at $720 \text{ }^{\circ}\text{C}$ had a negative effect on the mechanical properties. At higher stabilization temperatures, the YS was the same or even decreased with an increasing holding time (in the range of 280–297 MPa), which indicates significantly higher precipitation kinetics at these higher temperatures. At a stabilization temperature of $800 \text{ }^{\circ}\text{C}$, the YS decreased from 297 MPa at a hold of 1 h to 282 MPa at a hold of 10 h. The lowest YS values were found at a stabilization temperature of $900 \text{ }^{\circ}\text{C}$, where they reached values around 280 MPa. An increase in the YS with an increasing holding time was thus observed only at a stabilization

temperature of 720 °C. All HT modes reached significantly above-limit values of the YS at RT (min. 206 MPa requested).

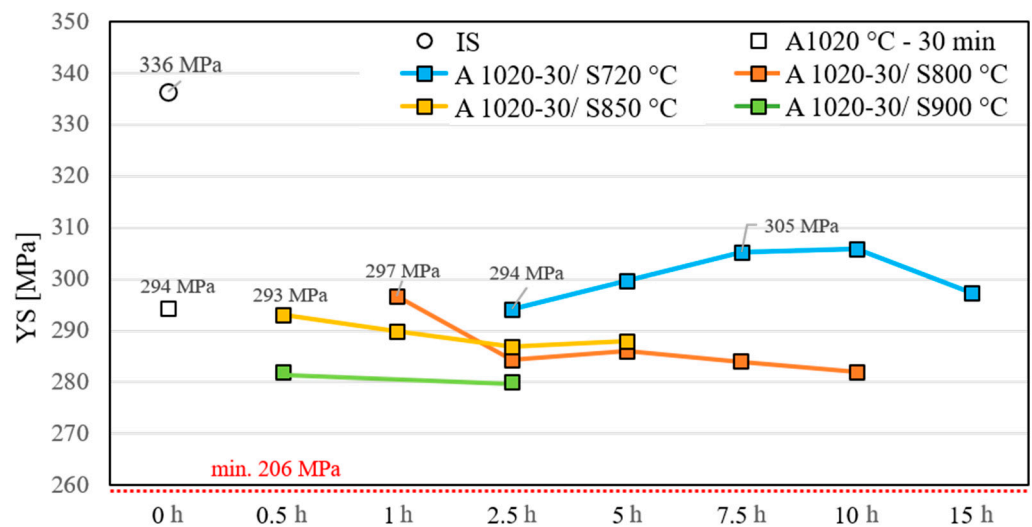


Figure 2. Development of YS after RT tensile test depending on the mode of heat treatment used. Samples after solution annealing (A), stabilization (A/S), and initial state (IS). The minimum required YS value at RT is marked in red.

Regarding the UTS, similar trends as for the YS were observed (Table 4). The ductility of all HT modes ranged between 52 and 54%. All the mechanical properties met the required limits for all processing modes.

3.2. Tensile Test at 350 °C

The UTS^{350 °C} of the initial state again reached visibly higher values than the other tested states (412 MPa). Even the samples processed only by the solution annealing achieved a relatively high UTS^{350 °C} of 398 MPa, i.e., slightly higher values than after stabilization. The UTS^{350 °C} of the stabilized samples ranged from 381 MPa to 395 MPa, while no significant differences were observed among the individual modes (Table 4). With an increasing holding time at the stabilization temperature, a very slightly decreasing trend was found at almost all temperatures. All the measured values, including for those samples after solution annealing, were above the limit (>353 MPa).

Very similar courses, with relatively small differences in the values, were also observed for the YS^{350 °C} (Table 4, Figure 3). The YS^{350 °C} of the initial state reached 277 MPa; after solution annealing with a duration of 30 min, a decrease in the YS^{350 °C} to 233 MPa was recorded. The YS values of the stabilized samples were in the range of 217–241 MPa. With an increasing holding time at the stabilization temperature, a gradual increase in the YS^{350 °C} during stabilization at 720 °C could be observed, with maximum holding times of 5 h and 10 h (241 MPa). The 7.5 h holding time showed a slight decrease to 235 MPa. At higher stabilization temperatures, a decrease in the YS^{350 °C} was recorded with longer temperature delays, indicating significantly faster kinetics of the precipitation processes. Even in this case, all regimes showed above-limit values of the YS^{350 °C} (>177 MPa). At a stabilization temperature of 800 °C, a decrease was found from 238 MPa, with a holding time of 1 h, to 225 MPa, with a holding time of 10 h. Again, the lowest YS^{350 °C} values were reached at a stabilization temperature of 900 °C, when values around 220 MPa were reached.

The ductility values of the stabilized samples then ranged between 29 and 34% (Table 4). In the initial state, lower ductility (26%) was observed, similar to solution annealing alone (27%).

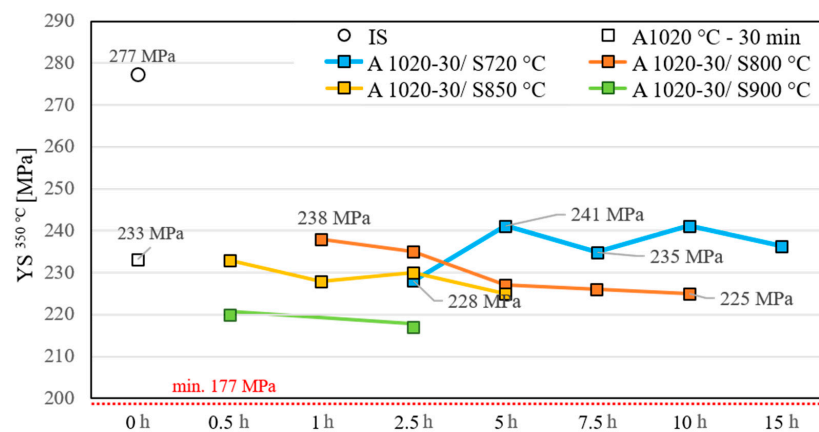


Figure 3. Development of $YS^{350^{\circ}\text{C}}$ depending on the mode of heat treatment used. Samples after solution annealing (A), stabilization (A/S), and initial state (IS). The minimum required $YS^{350^{\circ}\text{C}}$ is marked in red.

3.3. Metallography

The microstructure of all the samples was formed out of polyhedral austenite grains with coarser carbide particles at the grain boundaries. However, we focused mainly on the presence of intragranular precipitate. In the samples stabilized at 720 °C for 2.5 or 15 h, no significant differences were observed in the LM or SEM micrographs. Only after 10 h of holding at 800 °C was an increase in the density of fine particles inside the grains apparent (Figure 4). It can be assumed that with these parameters, a larger amount of secondary titanium carbonitrides inside the grains could have been precipitated and subsequently coarsened.

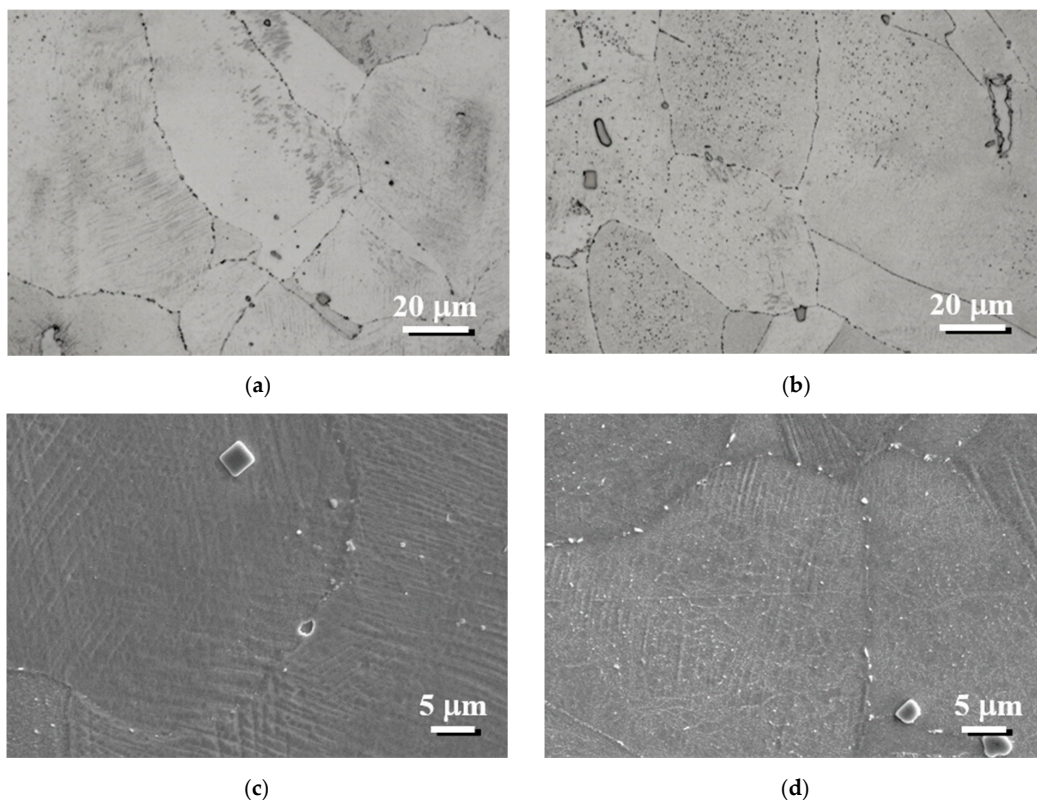


Figure 4. Images of microstructure of 08Ch18N10T steel after solution annealing at 1020 °C/30 min in combination with stabilization: 800 °C/1 h (a,c), 800 °C/10 h (b,d). LM micrographs (a,b) and SEM micrographs (c,d).

3.4. Transmission Electron Microscopy

Samples with a stabilization temperature of 800 °C and holding times of 1 h and 10 h were selected for TEM analysis. The results show that most of the grains of the austenitic matrix were divided by dislocation walls into subgrains. The dislocations in the subgrains formed a disordered dislocation network, and fine TiC carbide particles precipitated on them. At the grain boundaries, relatively coarse particles of chromium-rich $M_{23}C_6$ carbide and TiC carbide were identified using energy-dispersive X-ray microanalysis (EDX) and electron diffraction (Figure 5).

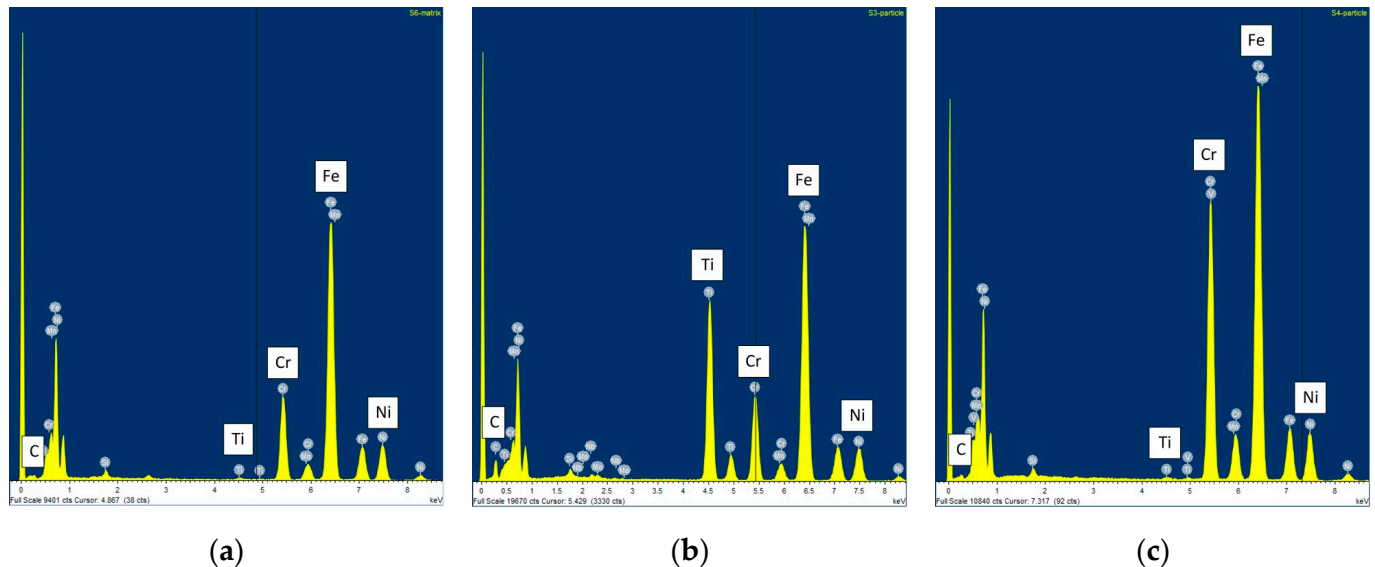


Figure 5. EDX spectra of matrix (a), titanium carbide (b), and chromium carbide (c) at the grain boundary in the sample stabilized at 800 °C for 1 h.

Particles of TiC carbides were observed in the sample stabilized for 1 h (Figures 6 and 7). Micrographs were acquired of the two-beam conditions, and carbides revealed a specific strain-field contrast typical for coherent precipitates [28–30]. At several different crystallographic orientations near the poles ([112], [221], and [114]), with one strong reflection type (220, 111, 420, or 311), the line of no contrast in the particle images was perpendicular to the diffraction vector with only a small deviation in a range of a few degrees caused by the anisotropic strain field in the matrix close to the particle interphase [28]. Two additional diffraction spots close to the strong reflection were always detected in the diffraction patterns; one corresponded to TiC carbide, and the other probably originated by diffraction on the compressed planes of the matrix. A bright-field image of such precipitates, together with the diffraction pattern, is shown in Figure 6. Austenitic grain appeared in the orientation near the pole [2–21], with a strong reflection, 220 γ . The same reflection type of the precipitate (220_{TiC}) and an extra spot of compressed matrix planes (220 _{γ -def}) are marked in the picture. It is known that TiC carbide precipitates in “cube-to-cube” orientation and, due to a large mismatch between the precipitate and the matrix lattice ($a_{\gamma} = 0.360$ nm, $a_{TiC} = 0.433$ nm), precipitation causes strong strain around the particles [31,32]. Some of the carbides were surrounded with dislocation loops to reduce the elastic strain in the matrix [33]. The diffraction patterns revealed a deviation of one or two degrees from the matrix orientation. The other observed particles seemed to be coherent in compliance with the bright-field image and diffraction patterns. Due to the deformation contrast, the image is significantly larger than the actual particle.

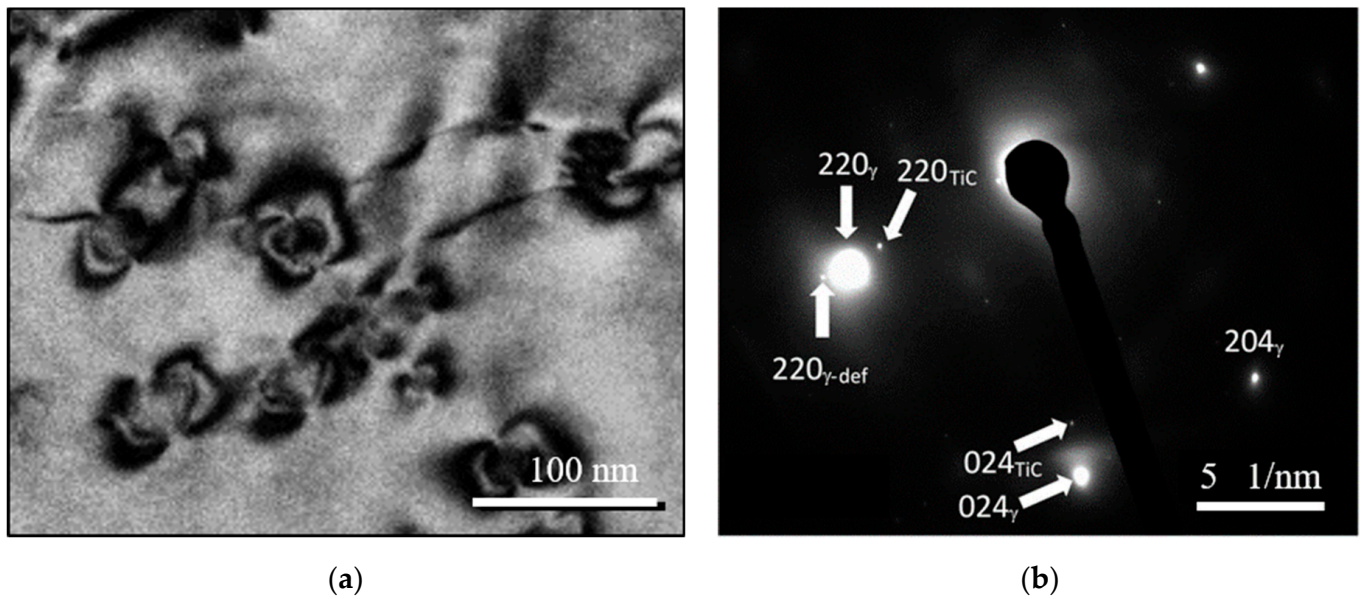


Figure 6. Sample stabilized for 1 h at 800 °C: (a) bright-field image of TiC precipitates and dislocations, (b) diffraction pattern of austenitic grain in orientation near the pole [2–21]. TEM micrographs.

A higher dislocation density and fine precipitate were observed in the sample with a 10 h hold (Figure 8) compared to the sample stabilized for 1 h (Figure 7). The particle density increased, and the particle bright-field images appeared smaller than in the sample stabilized for 1 h. The reason is the loss of coherence and the reduction of the elastic deformation of the matrix. The diffraction pattern showed that some TiC particles lost coherence during growth, and their lattice was rotated with respect to the matrix by more than 5°. Nevertheless, fine newly originated TiC carbides were still coherent, as shown in Figure 9.

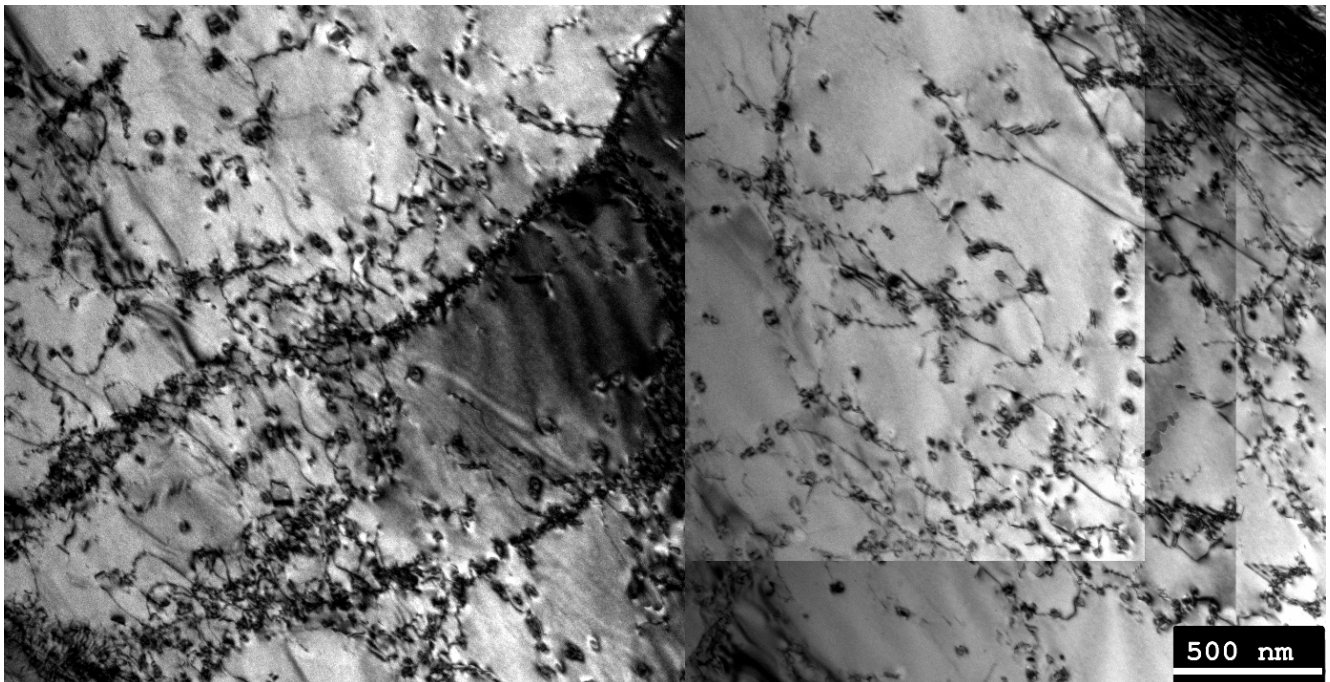


Figure 7. Sample stabilized at 800 °C for 1 h. Dislocation substructure of austenitic grain in orientation near the pole [112] with strong reflection type 111. TEM micrograph.



Figure 8. Sample stabilized at 800 °C for 10 h. Dislocation substructure of austenitic grain in orientation near the pole [001] with strong reflection type 200. TEM micrograph.

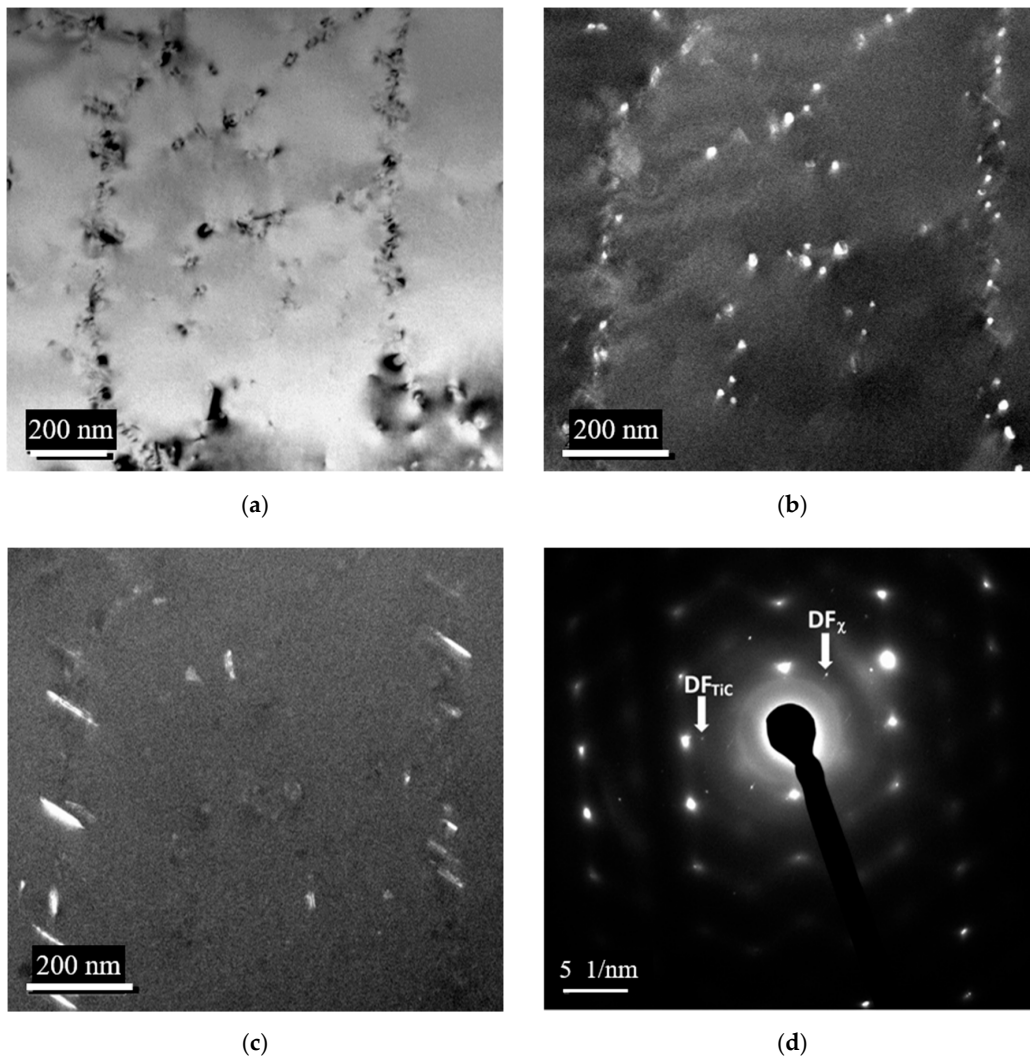


Figure 9. Cont.

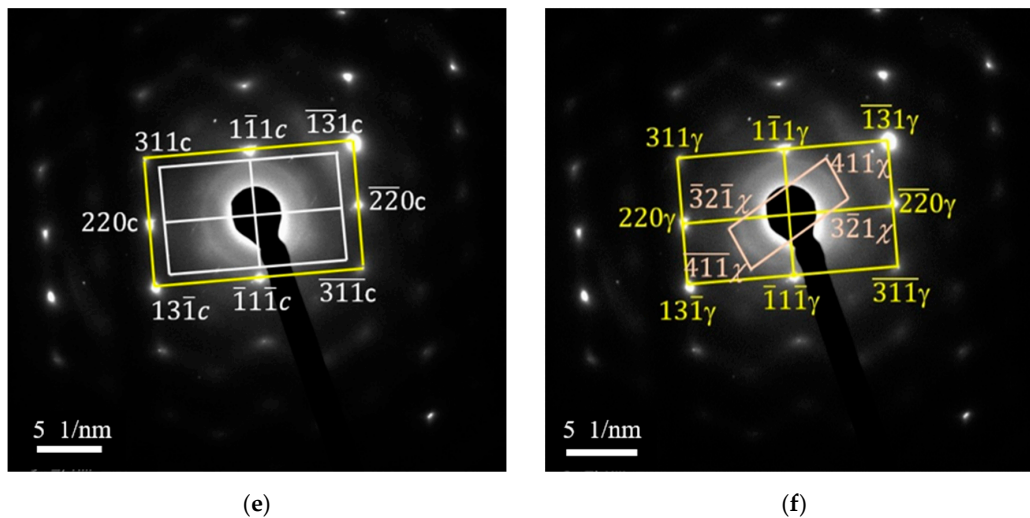


Figure 9. Sample stabilized at 800 °C for 10 h. Chains of fine precipitates along dislocations: (a) bright field, (b) dark field using reflection 220_{TiC} , (c) dark field using reflection 411_{χ} , (d) diffraction pattern with designated reflections of dark fields, (e) scheme of the matrix (yellow) and coherent precipitate (white) zones $[-112]$, (f) scheme of matrix (yellow) and χ -phase (pink) diffraction spots. TEM micrographs.

In addition, platelet-shaped particles clearly visible in the dark-field image were detected (Figure 9). According to the diffraction patterns, and in accordance with the literature, this was probably an intermetallic phase χ with the chemical formula $(Fe, Ni)_{36}Cr_{18}Mo_4$, which dissolves carbon and is sometimes referred to as $M_{18}C$ carbide [34]. Both types of particles nucleated along the subgrain boundaries.

4. Discussion

4.1. Assessment of the Proposed Heat Treatment Sequence

A heat treatment sequence involving solution annealing (SA) at 1020 °C with a hold of 30 min was designed for the experimental material. As the effective implementation of stabilization must be preceded by a suitably selected SA, increased attention was paid to this step. During a properly performed SA, sufficient dissolution of the intermediate phases and homogenization of the solid solution must take place. On the other hand, during solution annealing, it is not desirable to entirely eliminate deformation strengthening, which was achieved in the microstructure during the formation of the initial semi-finished product. It can be assumed that the energy stored in the microstructure in the form of deformation strengthening has a favorable effect on the kinetics of subsequent precipitation processes during HT. The annealing was therefore designed according to these findings and based on a study of the literature [35,36]. Research based on AISI 321 [24] gave an initial (dynamic) recrystallization temperature of 950 °C. At lower temperatures, only recovery (in this case, dynamic) occurs [37]. At temperatures above 1000 °C, a gradual increase in the grain size was observed [24,37].

Due to the fact that the initial semi-finished product for heat treatment was stabilized in the delivered condition, it is possible to assume a more difficult course of recrystallization processes (the fine precipitate anchor dislocations), and therefore, a temperature of 1020 °C was chosen for SA with a hold of 30 min.

The design of the stabilization regimes also used findings from similar research on AISI321 steel. Moura [38] stated that stabilization temperatures of up to 950 °C are effective (in terms of corrosion resistance). At lower stabilization temperatures (800–900 °C), an increase in the hardness of the structure was also observed. Research [39] dealing with the precipitation mechanisms and morphology of precipitates in the stabilization of AISI321 steel indicates precipitation temperatures of fine Ti (C, N) precipitate at 750–800 °C. These

precipitates significantly contribute to the overall strength of the steel. Based on these findings, stabilization temperatures in the range of 720–900 °C were proposed.

4.2. Assessment of the Effect of Stabilization Temperature and Hold

Lower stabilization temperatures in the range of 720–800 °C proved to be more suitable for achieving the required mechanical properties. At 720 °C, it was possible to observe a gradual increase in the strength characteristics with increasing dwell times (at RT as well as at 350 °C). After a 10 h hold, the highest values of strength and YS were reached. With a stabilization temperature of 800 °C, the trend was reversed—the highest values were observed at the shortest 1 h hold, and the mechanical properties continued to decrease with the holding time. Thus, it was possible to observe a clear dependence of the kinetics of precipitation of fine TiC carbides on the stabilization annealing temperature. At the lowest temperature (i.e., 720 °C) the carbides grew relatively slowly and stayed coherent for a longer period of time. The coherence is associated with a higher degree of precipitation hardening compared to the incoherent precipitates [40]. Because precipitation proceeds faster at higher temperatures, the maximum precipitation hardening by these particles shifted to shorter times as the stabilization annealing temperature increased. Along with the increasing stabilization temperature, lower maximum values of the strength characteristics were observed.

Diffraction analysis using TEM further examined the course of precipitation on selected samples stabilized at 800 °C with holds of 1 h and 10 h. Here, the precipitation of a very fine coherent precipitate was confirmed in the structure during a shorter dwell time (Figure 6). A larger amount of fine precipitate was observed in the 10 h sample, with some particles already losing coherence during growth (Figure 7). This proves the further precipitation of the precipitate and its coarsening during longer holds at the stabilization temperature. With the loss of coherence, the precipitation hardening with Ti(C, N) particles decreased. During longer annealing (10 h at 800 °C), incoherent platelet χ -phase particles (which can have a negative effect on the mechanical properties) also precipitated in the dislocation walls.

4.3. Assessment of the Effect of Repeated Heat Treatment

The results show that all modes of heat treatment compared to the initial state caused a decrease in the tensile strength and YS. Even when repeating the mode by which the as-delivered initial state was processed (i.e., SA at a temperature of 1020 °C and subsequent stabilization at 720 °C for 10 h), the achieved values were significantly lower (241 MPa vs. 277 MPa of the initial state). In addition, all stabilized samples (after repeated HT) showed above-limit values of all the required mechanical properties. In this case, two explanations are offered:

The heat treatment during the production process of the starting material had already largely depleted the energy stored in the material as a result of the previous forming, and thus, significantly affected the precipitation kinetics. On the one hand, the re-performed annealing promoted the precipitation processes by dissolving the alloying elements, and thus, achieved a certain supersaturation of the solid solution. On the other hand, high annealing temperatures could cause even better annealing of the remnants of the deformation structure. As a result, the course of precipitation was noticeably milder than that of the unheated forged material. The inconspicuous but relatively logical trends observed in the graphs in Figures 2 and 3 correspond to this.

The proposed 30 min holding time during SA was not long enough to dissolve the intermediate phases sufficiently (especially nitrides, which are very reluctant to dissolve), although this holding time was designed according to the literature and in consultation with Škoda JS, a.s. This fact is evidenced in particular by the values of the strength characteristics after SA, which were higher than the prescribed limits.

5. Conclusions

The experimental program was focused on describing the influence of stabilization parameters on heat-treated austenitic stainless steel 08Ch18N10T stabilized with titanium. The aim was also to design processing parameters that would guarantee the highest possible strength characteristics, especially the yield strength at 350 °C. A heat treatment was designed, including annealing at 1020 °C, with a hold of 30 min, and then a set of variants of stabilization at temperatures of 720 °C to 900 °C, with a holding time from 30 min to 15 h. Tensile testing found different trends in the development of the yield strength (at RT and 350 °C) depending on the stabilization temperature.

In principle, there were differences in the development of the strength characteristics among the stabilization temperatures of 720 °C and higher. At 720 °C, there was a gradual increase in the ultimate tensile strength and yield strength with an increasing holding time. The highest hot yield strength at this temperature was reached with holding times of 5 and 10 h (241 MPa). At higher temperatures (800 and 900 °C), the trend was reversed—the highest hot yield strengths were achieved with the shortest holds and decreased with longer holding times. The maximum hot yield strength for 800 °C stabilization (238 MPa) was achieved with the 1 h hold.

TEM microanalysis focusing on the fine Ti(C, N) precipitates showed that the precipitation kinetics increased significantly with increasing temperature. However, with a higher growth rate, there was also an earlier loss of coherence of the precipitates, which again caused a reduction in the solid solution strengthening. Therefore, for higher stabilization temperatures, it is necessary to set the holding time more carefully to achieve the desired result. In addition, in comparison to the stabilization temperature of 720 °C, it is necessary to take into account the slightly lower maximum achievable values of the strength characteristics at these higher temperatures (238 vs. 241 MPa). Therefore, these energy and time-saving processing modes can only be recommended for high-quality, thermo-mechanically processed semi-finished products.

Author Contributions: Conceptualization, T.J., Š.J. and H.J.; methodology, T.J., L.K. and D.J.; validation, H.J. and L.K.; formal analysis, L.K. and D.J.; investigation, T.J. and R.L.; resources: T.J., R.L. and H.J.; data curation, T.J.; writing—original draft preparation—T.J.; writing—review and editing Š.J. and H.J.; supervision, Š.J. and H.J.; project administration, T.J.; funding acquisition, Š.J. and H.J. All authors have read and agreed to the published version of the manuscript.

Funding: This research was funded by the student grant competition of the University of West Bohemia in Pilsen. The APC was funded by the SGS-2021-025 Application of electron beam melting for welding of advanced high-strength steels.

Data Availability Statement: The research data are not publicly available due to ongoing research.

Acknowledgments: The present contribution has been prepared with the support of the student grant competition of the University of West Bohemia in Pilsen and the SGS-2021-025 Application of electron beam melting for welding of advanced high-strength steels. The project was funded by specific resources of the state budget for research and development.

Conflicts of Interest: The authors declare no conflict of interest.

References

1. Lima, A.S.; Nascimento, A.M.; Abreu, H.F.G.; de Lima-Neto, P. Sensitization evaluation of the austenitic stainless steel AISI 304L, 316L, 321 and 347. *J. Mater. Sci.* **2005**, *40*, 139–144. [[CrossRef](#)]
2. Prepared under the Direction of the ASM International Handbook Committee. Metallurgy and properties of wrought stainless steels. In *ASM Specialty Handbook: Stainless Steels*, 1st ed.; Davis, J.R., Ed.; ASM International: Metals Park, OH, USA, 1994; p. 22.
3. ASM International. Prepared under the Direction of the ASM International Handbook Committee. In *ASM Handbook*; ASM International: Metals Park, OH, USA, 1992; Volume 3.
4. Gonçalves, R.B.; De Araújo, P.H.D.; Braga, F.J.V.; Terrones, L.A.H.; Paranhos, R.P.D.R. Effect of conventional and alternative solution and stabilizing heat treatment on the microstructure of a 347 stainless steel welded joint. *Weld. Int.* **2016**, *31*, 196–205. [[CrossRef](#)]

5. Gonzaga, A.; Barbosa, C.; Tavares, S.; Zeemann, A.; Payão, J. Influence of post welding heat treatments on sensitization of AISI 347 stainless steel welded joints. *J. Mater. Res. Technol.* **2019**, *9*, 908–921. [[CrossRef](#)]
6. Guan, K.; Xu, X.; Xu, H.; Wang, Z. Effect of aging at 700 °C on precipitation and toughness of AISI 321 and AISI 347 austenitic stainless steel welds. *Nucl. Eng. Des.* **2005**, *235*, 2485–2494. [[CrossRef](#)]
7. Sharma, A.; Prabhakar, V.; Sandhu, S.S. Microstructural characterization and mechanical performance along the thickness of electron beam welded stabilized AISI 321 stainless steel. *Met. Mater. Eng.* **2021**, *27*, 489–504. [[CrossRef](#)] [[PubMed](#)]
8. Mahmoudi, A.; Esmailian, M.; Aghamiri, S.E. Effect of Stabilizing Heat Treatment on Intergranular Corrosion Resistance of Welded Stainless Steel AISI 321. *Adv. Mater. Res.* **2012**, *535–537*, 692–696. [[CrossRef](#)]
9. Pardo, A.; Merino, M.; Coy, A.; Viejo, F.; Carboneras, M.; Arrabal, R. Influence of Ti, C and N concentration on the intergranular corrosion behaviour of AISI 316Ti and 321 stainless steels. *Acta Mater.* **2007**, *55*, 2239–2251. [[CrossRef](#)]
10. Morshed-Behbahani, K.; Najafisayar, P.; Pakshir, M.; Shahsavari, M. An electrochemical study on the effect of stabilization and sensitization heat treatments on the intergranular corrosion behaviour of AISI 321H austenitic stainless steel. *Corros. Sci.* **2018**, *138*, 28–41. [[CrossRef](#)]
11. Kopylov, V.I.; Nokhrin, A.V.; Kozlova, N.A.; Chegurov, M.K.; Gryaznov, M.Y.; Shotin, S.V.; Melekhin, N.V.; Tabachkova, N.Y.; Smetanina, K.E.; Chuvil' deev, V.N. Effect of σ -Phase on the Strength, Stress Relaxation Behavior, and Corrosion Resistance of an Ultrafine-Grained Austenitic Steel AISI 321. *Metals* **2022**, *13*, 45. [[CrossRef](#)]
12. Fekete, B.; Kasl, J.; Jandova, D.; Jóni, B.; Misják, F.; Trampus, P. Low cycle thermomechanical fatigue of reactor steels: Microstructural and fractographic investigations. *Mater. Sci. Eng. A* **2015**, *640*, 357–374. [[CrossRef](#)]
13. Jandová, D.; Fekete, B.; Kasl, J.; Bertalan, J. Microstructure of 08ch18n10t austenitic steel after thermo-mechanical fatigue tests. In Proceedings of the 24th International Conference on Metallurgy and Materials, Brno, Czech Republic, 3–5 June 2015.
14. Chen, H.; Li, W.; Chen, W.; Chen, J.; Zhang, S. Influence of prior creep-fatigue exposure on remnant tensile and creep properties of AISI 321 austenite stainless steel. *Int. J. Fatigue* **2022**, *159*, 106826. [[CrossRef](#)]
15. Tiamiyu, A.A.; Eduok, U.; Szpunar, J.A.; Odeshi, A.G. Corrosion behavior of metastable AISI 321 austenitic stainless steel: Investigating the effect of grain size and prior plastic deformation on its degradation pattern in saline media. *Sci. Rep.* **2019**, *9*, 12116. [[CrossRef](#)] [[PubMed](#)]
16. Li, W.; Chen, H.; Li, C.; Huang, W.; Chen, J.; Zuo, L.; Ren, Y.; He, J.; Zhang, S. Microstructure and tensile properties of AISI 321 stainless steel with aluminizing and annealing treatment. *Mater. Des.* **2021**, *205*, 109729. [[CrossRef](#)]
17. Yang, X.; Yu, C.; Yang, X.; Yan, K.; Qian, G.; Wang, B.; Yan, W.; Shi, X. Microstructure and mechanical properties of an austenitic heat-resistance steel after service at 570 °C and 25.4 MPa for 18 years. *J. Mater. Eng. Perform.* **2021**, *30*, 1030–1038. [[CrossRef](#)]
18. Jirková, H.; Janda, T.; Růžička, J.; Mach, J.; Volkmannová, J. Effect of holding time at stabilization annealing on properties of 08CH18N10T austenitic stainless steel. In Proceedings of the 29th International Conference on Metallurgy and Materials, Brno, Czech Republic, 20–22 May 2020.
19. Radionova, L.V.; Perevozchikov, D.V.; Makoveckii, A.N.; Eremin, V.N.; Akhmedyanov, A.M.; Rushchits, S.V. Study on the Hot Deformation Behavior of Stainless Steel AISI 321. *Materials* **2022**, *15*, 4057. [[CrossRef](#)]
20. Zhao, D.; Ren, L.; Wang, Y.; Wang, W.; Zhu, Z.; Fu, W. Hot Deformation Behaviors of as Cast 321 Austenitic Stainless Steel. *Metals* **2021**, *11*, 1245. [[CrossRef](#)]
21. Anoop, C.R.; Singh, R.K.; Kumar, R.R.; Miyala, J.; Murty, S.N.; Tharian, K.T. Development and Validation of Processing Maps for Hot Deformation of Modified AISI 321 Austenitic Stainless Steel. *Mater. Perform. Charact.* **2020**, *9*, 150–169. [[CrossRef](#)]
22. Litovchenko, I.; Akkuzin, S.; Polekhina, N.; Almaeva, K.; Moskvichev, E. Structural Transformations and Mechanical Properties of Metastable Austenitic Steel under High Temperature Thermomechanical Treatment. *Metals* **2021**, *11*, 645. [[CrossRef](#)]
23. Jirkova, H.; Janda, T.; Peković, M.; Říha, J.; Mach, J.; Krsová, D. Influence of rolling speed during hot forming using HDQT-R 30-12 machine on the properties of stainless steel 08Ch18N10T. In Proceedings of the IOP Conference Series: Materials Science and Engineering, Pilsen, Czech Republic, 30 November–4 December 2020.
24. Podaný, P.; Martínek, P.; Nacházel, J.; Balcar, M. Heat Treatment of Reactor Vessel Steel 08Ch18N10T. In Proceedings of the Materials Science and Technology Conference and Exhibition, Pittsburg, PA, USA, 7–11 October 2012.
25. GOST 1497-84; Metals. Methods of Tension Test. USSR: USSR State Committee for Standards, 1986. Available online: <https://auremo.biz/gosts/gost-1497-84.html> (accessed on 9 April 2023).
26. GOST 9651-84; Methods of Tension Test at Elevated Temperature. USSR: USSR State Committee for Standards, 1986. Available online: <https://auremo.biz/gosts/gost-9651-84.html> (accessed on 9 April 2023).
27. EN ISO 6892-1; Metallic Materials–Tensile Testing–Part 1: Method of Test at Room Temperature. Praha: Czech Standardization Agency: 2021. Available online: <https://www.iso.org/obp/ui/#iso:std:iso:6892:-1:ed-3:v1:en> (accessed on 9 April 2023).
28. Degischer, H.P. Diffraction contrast from coherent precipitates in elastically-anisotropic materials. *Philos. Mag.* **1972**, *26*, 1137–1151. [[CrossRef](#)]
29. Dahmen, U. Transmission electron microscopy characterization of precipitates. *Ultramicroscopy* **1989**, *30*, 102–115. [[CrossRef](#)]
30. Liu, C.; Li, Y.; Zhu, L.; Shi, S. Effect of coherent lattice mismatch on the morphology and kinetics of ordered precipitates. *J. Mater. Eng. Perform.* **2018**, *27*, 4968–4977. [[CrossRef](#)]
31. Hazotte, A.; Racine, A.; Denis, S. Internal mismatch stresses in nickel superalloys: A finite element approach. *J. Phys. IV* **1996**, *6*, C1-119–C1-128. [[CrossRef](#)]

32. Andrén, H.O.; Henjered, A.; Nordén, H. Composition of MC precipitates in a titanium stabilized austenitic stainless steel. *J. Mater. Sci.* **1980**, *15*, 2365–2368. [[CrossRef](#)]
33. Sampath, S.; Janisch, R. Ab initio prediction of the critical thickness of a precipitate. *J. Phys. Condens. Matter* **2013**, *25*, 355005. [[CrossRef](#)]
34. Escriba, D.; Materna-Morris, E.; Plaut, R.; Padilha, A. Chi-phase precipitation in a duplex stainless steel. *Mater. Charact.* **2009**, *60*, 1214–1219. [[CrossRef](#)]
35. Prepared under the Direction of the ASM International Handbook Committee. Heat treating of stainless steels. In *ASM Handbook: Volume 4: Heat Treating*, 3rd ed.; ASM International: Metals Park, OH, USA, 1995; pp. 1694–1702.
36. Prepared under the Direction of the ASM International Handbook Committee. Austenitic stainless steels. In *Heat Treater's Guide: Practices and Procedures for Irons and Steels*, 2nd ed.; Chandler, H., Ed.; ASM International: Metals Park, OH, USA, 1995; p. 752.
37. Ghazani, M.S.; Eghbali, B. Characterization of the hot deformation microstructure of AISI 321 austenitic stainless steel. *Mater. Sci. Eng. A* **2018**, *730*, 380–390. [[CrossRef](#)]
38. Moura, V.; Kina, A.Y.; Tavares, S.S.M.; Lima, L.D.; Mainier, F.B. Influence of stabilization heat treatments on microstructure, hardness and intergranular corrosion resistance of the AISI 321 stainless steel. *J. Mater. Sci.* **2007**, *43*, 536–540. [[CrossRef](#)]
39. Smola, B. Precipitation and hardening mechanisms in the AISI 321 steel. *Acta Univ. Carolinae. Math. Et Phys.* **1990**, *31*, 27–46.
40. Wang, Q.; Li, Z.; Pang, S.; Li, X.; Dong, C.; Liaw, P.K. Coherent precipitation and strengthening in compositionally complex alloys: A review. *Entropy* **2018**, *20*, 878. [[CrossRef](#)] [[PubMed](#)]

Disclaimer/Publisher's Note: The statements, opinions and data contained in all publications are solely those of the individual author(s) and contributor(s) and not of MDPI and/or the editor(s). MDPI and/or the editor(s) disclaim responsibility for any injury to people or property resulting from any ideas, methods, instructions or products referred to in the content.